SODANKYLÄ GEOPHYSICAL OBSERVATORY
PUBLICATIONS

OULUN YLIOPISTO
UNIVERSITY of OULU
1958 ▪▪▪ 2008

No. 102

IONOSPHERIC D-REGION STUDIES BY MEANS OF ACTIVE HEATING EXPERIMENTS AND MODELLING

ANTTI KERO

Oulu 2008

SODANKYLÄ GEOPHYSICAL OBSERVATORY
PUBLICATIONS

OULUN YLIOPISTO
UNIVERSITY of OULU
1958 ▪▪▪ 2008

No. 102

IONOSPHERIC D-REGION STUDIES BY MEANS OF ACTIVE HEATING EXPERIMENTS AND MODELLING

ANTTI KERO

Academic Dissertation to be presented, with the permission of the Faculty of Science of the University of Oulu, for public discussion in Polaria, Sodankylä, on 8th December, 2008, at 12 o'clock noon.

Oulu 2008

SODANKYLÄ GEOPHYSICAL OBSERVATORY PUBLICATIONS
Editor: Johannes Kultima
Sodankylä Geophysical Observatory
FIN-99600 SODANKYLÄ, Finland

This publication is the continuation of the former series
"Veröffentlichungen des geophysikalischen Observatoriums
der Finnischen Akademie der Wissenschaften"

Sodankylä Geophysical Observatory
Publications

ISBN 978-951-42-8915-6
ISSN 1456-3673

OULU UNIVERSITY PRESS
Oulu 2008

Abstract

Powerful radio waves can heat an electron gas via collisions between free electrons and neutral particles. Since the discovery of the Luxembourg effect in 1934, this effect is known to take place in the D-region ionosphere. According to theoretical models, the EISCAT Heating facility is capable of increasing the electron temperature by a factor of 5–10 in the D region, depending mostly on the electron density profile. Various indirect evidence for the existence of the D-region heating effect has been available, including successful modification of ionospheric conductivities and mesospheric chemistry. However, an experimental quantification of the electron temperature at its maximum in the heated D-region ionosphere has been missing. In particular, incoherent scatter (IS) radars should be able to observe directly plasma parameters, such as the electron temperature, although the heated D-region ionosphere is not a trivial target because of low electron density, and hence, small signal-to-noise ratio (SNR).

In this thesis, Papers I and III present unique estimates for heated D-region electron temperatures based on IS measurements. It turned out that the theoretical predictions of the electron temperature generally agree with the few existing observations, at least at the altitudes of the maximum heating effect.

Quite in contrast, when the D-region heating effect on the cosmic radio noise absorption was verified for the first time by the statistical data analysis presented in Paper II, the absorption enhancements due to heating were found to be an order of magnitude smaller than model results. The reason for this discrepancy remains still as open question, although one possible explanation is provided by the electron-temperature dependent ion chemistry, which was not taken into account in the modelling. The significance of the heating-induced ion chemistry effect in the D-region was investigated in Paper IV. There the heating-induced negative ion formation is proposed as a potential explanation for the observed modulation of Polar Mesosphere Winter Echo (PMWE) power.

Acknowledgements

I thank Sodankylä Geophysical Observatory for hosting me during this thesis work. I feel privileged for having the opportunity to work in this inspiring research environment based on nearly 100-years of heritage of geophysical measurements. Thanks are due to the whole SGO staff for making my work here a pleasant experience.

In addition to financial support provided by SGO, I am grateful to the Academy of Finland and the Thule Institute for funding this work.

Special thanks to my supervisors Esa Turunen and Tilmann Bösinger for their advice and encouragement. I highly appreciate that I have been able to collaborate with colleagues and co-authors Thomas Ulich, Carl-Fredrik Enell, Juha Vierinen and Ilkka Virtanen, who have helped me in uncountable ways.

I thank Mike Kosch and Björn Gustavsson for their valuable referee comments.

This work is dedicated to my daughter Sanni. She's my pride and joy.

Contents

Prologue

In recent years, there has been a growing scientific interest on the altitudes of the mesosphere and the lower thermosphere, i.e. the D-region ionosphere (50-100 km). This research is largely motivated by an acute need for better understanding of the coupling between the upper atmosphere and the climate system. For instance, several studies have shown that the solar particle forcing on the coupled ion and neutral chemistry in the D region leads to formation of odd nitrogen and odd hydrogen compounds, which can reduce significantly the ozone content in the mesosphere and stratosphere [e.g. Randall et al., 1998; Seppälä et al., 2007; Lopéz-Puertas et al., 2005]. This process takes place especially inside the polar vortex, where the air mass is isolated and transported downward. According to some models, the ozone change due to this process is capable of changing the atmospheric circulation and causing significant anomalies in ground temperatures [Rozanov et al., 2005]. Most recently, these anomalies are verified by temperature records [Seppälä et al., 2008].

The climate predictions by the IPCC [2007] are based on models which ignore the poorly known solar particle forcing. This might not be justified in the future. Besides the solar particle input, there is also a variety of other poorly understood phenomena, such as transient luminous events [Enell et al., 2008a] and meteoric forcing on the atmosphere [Gabrielli et al., 2004], which might be important – or just interesting.

In this thesis, traditional radio wave methods, such as incoherent scatter radar experiments, riometer measurements and HF heating experiments, are used for remote sensing of the D region in advanced ways, combining novel experimental methods with a detailed modelling approach. Especially, the active heating effect on the D-region ion chemistry is considered. This work is part of the research conducted in the Aeronomy Unit of the Sodankylä Geophysical Observatory (SGO) concentrating on the altitudes of the mesosphere and the lower thermosphere.

Outline of this thesis

After a short historical perspective and an overview on current scientific topics related to active radio wave heating experiments, the objectives of this study are listed in Chapter 1. Basic principals of both experimental and theoretical tools used in the research are concerned in Chapters 2 and 3. The central results are reviewed in Chapter 4 and summarised in Chapter 5, where their potential significance and impact on future investigations are addressed.

The thesis is based upon the following four papers, which in the text will be

referred to by their Roman numerals:

I Kero, A., T. Bösinger, P. Pollari, E. Turunen, and M. Rietveld, First EISCAT measurement of electron-gas temperature in the artificially heated D-region ionosphere, *Ann. Geophys.*, *18*, 1210–1215, 2000. (©2000 by EGS-Springer-Verlag. Reprinted with permission.)

II Kero, A., C.-F. Enell, Th. Ulich, E. Turunen, M. T. Rietveld, and F. H. Honary. Statistical signature of active D-region HF heating in IRIS riometer data from 1994-2004, *Ann. Geophys.*, *25*, 407–415, 2007. (©2007 by the European Geosciences Union. Reprinted with permission.)

III Kero, A., J. Vierinen, C.-F. Enell, I. Virtanen, and E. Turunen, New incoherent scatter diagnostic methods for the heated D-region ionosphere, *Ann. Geophys.*, *26*, 2273–2279, 2008. (©2007 by the European Geosciences Union. Reprinted with permission.)

IV Kero, A., C.-F. Enell, A. Kavanagh, J. Vierinen, I. Virtanen, and E. Turunen, Could negative ion production explain the Polar Mesosphere Winter Echo (PMWE) modulation in active HF heating experiments?, *Geophys. Res. Lett.*, submitted, 2008. (©2008 by the American Geophysical Union. Reprinted with permission.)

Firstly, the D-region electron temperature enhancement due to heating is quantified for the first time by incoherent scatter measurements in Papers I and III. In these investigations, the presented data analysis generally agrees with the theoretical D-region heating modelling introduced in Section 3.3. However, there is a significant disagreement between the detailed modelling of the heating effect on the cosmic radio noise absorption and the statistical effect found in the IRIS riometer data (Paper II). This dilemma remains still, although taking into account the heating effect on the ion chemistry might explain, at least partially, the discrepancy as shown in Section 4.2. Finally in Paper IV, a heating effect on the negative ion chemistry is proposed as a new possible mechanism causing the heater-induced PMWE modulation.

Contributions

All Papers I-IV are based on my initial ideas, the research was conducted according to my vision and the papers are written mostly by myself as a first author. On the other hand, the research work was always done in close co-operation with the other authors, whose contributions are acknowledged in the following.

The research published in Paper I was conducted under supervision of Tilmann Bösinger. The actual heating experiments were carried out by Michael Rietveld together with me, while the VHF radar was operated by Thomas Ulich. Finally, I did the modelling and the data analysis in a close collaboration with Päiviö Pollari and Esa Turunen.

Paper II was done in SGO under supervision of Esa Turunen. Thomas Ulich introduced some statistical methods used and Carl-Fredrik Enell helped me editing the manuscript, as well as the following articles. Other co-authors provided detailed specifications of the instruments (EISCAT Heating and IRIS riometer) for the modelling

and access to the data for the statistical survey. In addition, all the co-authors made valuable remarks on the topic during the writing process.

Measurements presented in Papers III and IV are based on novel radar methods developed by the Inverse Problems group of SGO, lead by Markku Lehtinen. The radar transmission used in the experiment was coded by Ilkka Virtanen, who also made the raw analysis for the data. Juha Vierinen made a remarkable contribution in the subsequent data analysis by applying the MCMC method in Paper III. Carl-Fredrik Enell did several state-of-art ion chemistry model runs as an essential contribution to Papers III and IV. Andrew Kavanagh helped me to write the extended introduction of Paper IV.

Chapter 1

Introduction

1.1 A brief historical perspective

Marconi's famous transatlantic radio transmission from Cornwall to New Foundland in 1901 led to the experimental discovery of an electrically conducting upper atmosphere, later named ionosphere, which could act as a reflector for radio waves. The theory of radio wave propagation in such a medium, i.e. a cold magnetised plasma containing free electrons and ions, was developed by Appleton among others in late 1920s. The theory predicts that radio waves reflect from an altitude where the natural plasma oscillations match the radio wave frequency. This makes it possible to probe the altitude profile of the ionosphere by measuring the time delay between the transmission and the reflected wave reception for radio waves at different frequencies. This so-called *ionosonde* technique was one of the first radar applications, and it is still in use on routine basis. Early ionosonde soundings revealed that the ionosphere consists of multiple stratified reflection regions instead of a single mirroring layer. Appleton denoted these regions by letters D, E and F in his experiments and this nomenclature still remains.

This study concentrates on the lowest part of the ionosphere, the D region, located in altitudes of 50-100 km. Characteristic for this region is a high collision rate between the plasma components. The theory of radio wave propagation predicts that by collisions between free electrons and neutral particles, a part of the radio wave energy is absorbed by the plasma. The absorbed energy is transferred into thermal energy of electrons.

The so-called *Luxembourg effect* was the first experimental indication of the powerful radio waves' capability to heat the ionosphere. Tellegen [1933] reported that the AM radio broadcast of the Luxembourg station could be heard at Eindhoven in the background of a programme transmitted from Beromünster at a different frequency. Bailey and Martyn [1934] suggested that the powerful Luxembourg station, located between the transmitter at Beromünster and the receiver at Eindhoven, modified the ionospheric radio wave propagation path by heating the electron gas. This finding can be regarded as the first active heating experiment, although an unintended one.

After the Second World War, scientists started to explore radio wave heating

techniques for modifying ionospheric conditions. The first megawatt-range heating facilities were built in the 1970s (Platteville, Colorado, USA and SURA, Novgorod, USSR). Especially the usage of a periodically heated ionosphere as a large-scale antenna for electromagnetic wave generation at low frequencies was studied extensively. In the USA as well as the former USSR, this research was motivated by the military requirement to communicate with deeply submerged submarines, although in practise, the capability of heating facilities for this purpose turned out to be insufficient [Barr, 1998]. However, scientific usage of active heating techniques expanded to various fields, some of them introduced in Section 1.2. New facilities were built for these purposes in the 1980s (Arecibo, Puerto Rico, USA; Tromsø, Norway; HIPAS, Alaska, USA) and most recently HAARP in Alaska, USA (1995) and SPEAR in Svalbard (2003).

1.2 Heating experiments today

Some central research topics related to active heating experiments are briefly discussed in the following.

Plasma instabilities In contrast to the heating mechanism in the collisional plasma of the D-region ionosphere, the heating effects in the E and F regions take place in resonance conditions, where the radio wave oscillation feeds energy to the ambient plasma via non-linear positive feedback processes. *Parametric decay instability*, sometimes called *three-wave instability* or *Langmuir turbulence*, is developed when the radio wave forms a positive feedback loop with Langmuir and ion-acoustic waves. *Thermal resonance instability* takes place when the upper hybrid resonance condition is met: $\omega^2 = \omega_p^2 + \Omega_e^2$, where ω, ω_p and Ω_e denote angular frequency of the radio wave, plasma frequency and the electron gyro frequency, respectively. Manifestations of these mechanisms are monitored by coherent and incoherent scatter radars [e.g., Stubbe et al., 1984; Rietveld et al., 2002], as well as optical observations.

Artificial optical emissions Heater-induced plasma turbulence is responsible for artificial optical emissions similar to natural aurora [e.g. Brändström et al., 1999]. These emissions originate typically slightly below the reflection altitude and their intensity maximises sharply near the magnetic zenith direction. The brightest emissions are O(^{1}D) 630 nm in the F region and O(^{1}S) 557.7 nm in the E region. [Kosch et al., 2007].

ULF-VLF waves The electric conductivity of a collisional plasma depends on the prevailing electron-neutral collision frequency, i.e. on the electron temperature. The timescale of the heater-induced electron temperature change in D-region altitudes varies from a few microseconds to milliseconds. The fast response makes it possible to use the heated area as a large-scale transmitting antenna for electromagnetic waves in the ELF–VLF frequency range by altering the natural ionospheric current system periodically via the conductivity. Barr [1998] reviews the development of this method starting from the first successful experiment by Getmatsev et al. [1974]. In addition

to the fast modification of the collision-rate, the electron-temperature dependent ion chemistry affects the electron density, and hence also the conductivity, on timescales of seconds. This provides a tool for generating magnetic pulsations in the ULF frequency range [Stubbe, 1996].

Coherent mesospheric scattering Strong radar echoes from a narrow altitude range near the polar summer mesopause have become a familiar feature in radar observations across a range of frequencies [e.g., Ecklund and Balsley, 1981; Karashtin et al., 1997; Röttger et al., 1988, 1990]. These so-called *polar mesosphere summer echoes* (PMSE) are caused by coherent Bragg-scattering from small-scale turbulence structures. The existence of these irregularities relies on slow diffusion provided by charged aerosol particles [Rapp and Lübken, 2004]. Both, the diffusion of the electrons and the charging of the aerosols, depend on the electron temperature, which makes it possible to modify the reflectivity of the PMSE by means of heating experiments [e.g., Chilson et al., 2000; Belova et al., 2003]. The characteristic response of the PMSE backscattered power to heating, including a special overshoot effect when the heater is turned off, reveals properties of the charged particles [e.g., Havnes, 2004; Chen and Scales, 2005; Scales and Chen, 2008].

Strong radar echoes from the winter polar mesosphere, *polar mesosphere winter echoes* (PMWE), were first observed in the 1980s in Alaska [Ecklund and Balsley, 1981; Balsley et al., 1983] and Norway [Czechowsky et al., 1989]. Competing theories coexist over the cause of PMWE with the two principal contenders either relying on turbulence from breaking gravity waves [Lübken et al., 2006] or the effects of highly-damped ion-acoustic waves generated by partial reflection of infrasonic waves [Kirkwood et al., 2006]. Kavanagh et al. [2006] made the first observations of PMWE being modulated by high-power heating. In Paper IV, heating-induced negative ion production is suggested to play an important role in the PMWE modulation.

In addition to the natural mesospheric coherent echoes, a method for generating artificial coherent backscattering from the ionosphere was developed in Russia already in 1975 [Belikovich et al., 2002]. In this approach, *artificial periodic irregularities* (API), which are formed by the action of a standing wave structure between the upcoming and the reflected heater radio wave, are probed with short pulses transmitted from the heater and received by ionosonde. In the mesosphere, the small-scale electron density gradients are caused by the electron-temperature dependent negative ion chemistry.

1.3 Scientific questions addressed in this thesis

The main objective of this thesis is to verify, for the first time, the electron temperature enhancement in the D-region ionosphere due to active radio wave heating. Papers I-III are devoted to this problem. Secondly, the heating effect on the daytime D-region ion chemistry is investigated in Papers III and IV. Experimental and theoretical tools described in the following Chapters 2 and 3 are utilised to tackle these problems.

Chapter 2

Instruments

The heating effects are investigated by a full arsenal of experimental techniques applied to the upper atmosphere and near space research. The ground based instrumentation consists of UHF, VHF and HF radars, ionosondes (API technique), riometers (e.g. IRIS), ULF-VLF receivers and optical instruments (cameras and photometers). Besides the ground based methods, satellite borne instruments are also frequently used for investigations of heating-induced effects.

However, this study concentrates on the combined EISCAT Heating and VHF radar experiments in Papers I, III and IV. In Paper II, a ten-year record of the past EISCAT heating experiments is used for detecting a statistical D-region heating effect on the cosmic radio noise absorption observed by the Kilpisjärvi IRIS riometer. A short technical overview of these facilities is presented in the following.

2.1 EISCAT facilities

EISCAT (European Incoherent SCATter) is an international research organisation operating incoherent scatter radars in Northern Scandinavia. It is funded and operated by the research councils of the EISCAT associate countries, currently Norway, Sweden, Finland, Japan, China, the United Kingdom. The mainland transmitter/receiver site for the UHF (931 MHz) and VHF (224 MHz) radars [Folkestad et al., 1983] is located at Ramfjordmoen (69.59° N, 19.23° E), close to the city of Tromsø, in Norway. In addition, there are remote UHF receiver stations located in Sodankylä (67.36° N, 26.63° E), Finland, and Kiruna (67.86° N, 20.44° E), Sweden, making it possible to measure the target velocity vector components in a common scattering volume of the receiver antenna beams. The EISCAT Heating facility [Rietveld et al., 1992] is located at Tromsø, next to the IS radars (see Fig. 2.1). The EISCAT Svalbard Radar (ESR), located on the island of Spitsbergen (78.15° N, 16.03° E), consist of two parabolic dish antennas operating at 500 MHz [Wannberg et al., 1997]. The next generation EISCAT IS radar system, based on the phased array technique, is currently under development.

The VHF radar was selected for monitoring the D-region ionosphere during the heating experiments described in Papers I, III and IV due to the longer radar wavelength (1.338 m for VHF, 0.3229 m for UHF) and therefore a stronger backscattered signal.

The EISCAT VHF antenna is a parabolic cylinder including 128 cross-dipole antennas along the focal line of the reflector. This setup produces a beam of 0.6° in EW and 1.7° in NS direction, confined by both the reflector and phasing of the radiation elements. The antenna gain is 46 dB with respect to an isotropic radiator. The power for the antenna is generated by a special designed klystron, which has a peak power of 1.5 MW. The maximum duty cycle, i.e. the fraction of time the transmitter can operate at full power, is 12.5%. Hence the transmitted signal is divided into phase coded pulses. Usage of the phase coded transmissions allow the radar to be operated at high duty cycle and still produce range resolutions much shorter than the pulse length used. In fact, Lehtinen [1989] has shown, that the optimal pulse length is equal to 1.5 times the desired range resolution. Since the IS signal is generally very weak, some sophisticated coding techniques have been developed for optimising the SNR of the experiments [see e.g. Lehtinen et al., 2008].

The radar receiver system consists of several stages of signal amplifiers and mixers enabling the VHF signal sampling in the end by an AD converter [Folkestad et al., 1983]. Traditionally, a hardware correlator unit is used for calculating the autocorrelation function (ACF) estimates based on the digital samples. However, in the measurements shown in Papers III and IV, the transmitted and received pulses are sampled directly and the ACF estimates are obtained by means of statistical inversion [Virtanen et al., 2007].

The full technical description of the VHF system is available in Folkestad et al. [1983] and Hagfors et al. [1982]. The principle of the incoherent scatter data analysis based on the measured ACF is presented in Section 3.4.

EISCAT Heating facility [Rietveld et al., 1992] is located at the EISCAT mainland transmitter site, next to the UHF and VHF radars (see Fig. 2.1). The heater consists of 12 power amplifiers of 100 kW nominal power and three phased arrays of crossed dipole antennas, later referred to as EISCAT Heating Antennas 1, 2 and 3. Crossed dipoles are used for generating one of the two circular polarisations, later called O-mode and X-mode corresponding to the left- and righthanded direction of the radio wave electric field rotation, respectively.

Operational frequency ranges of Antennas 1 and 2 are 5.4–8.0 MHz and 3.8–5.7 MHz, respectively. Antenna 3 (5.4–8.0 MHz) has been converted for receiving only. For maximal effective radiation power (ERP), Antenna 1 is used for the dedicated D-region heating experiments presented in Papers I, III and IV. The antenna field of 12x12 crossed dipoles provides approximately 28 dB gain, and 600 MW effective radiation power (with respect to an isotropic radiator) at the lowest licensed frequency of 5.423 MHz.

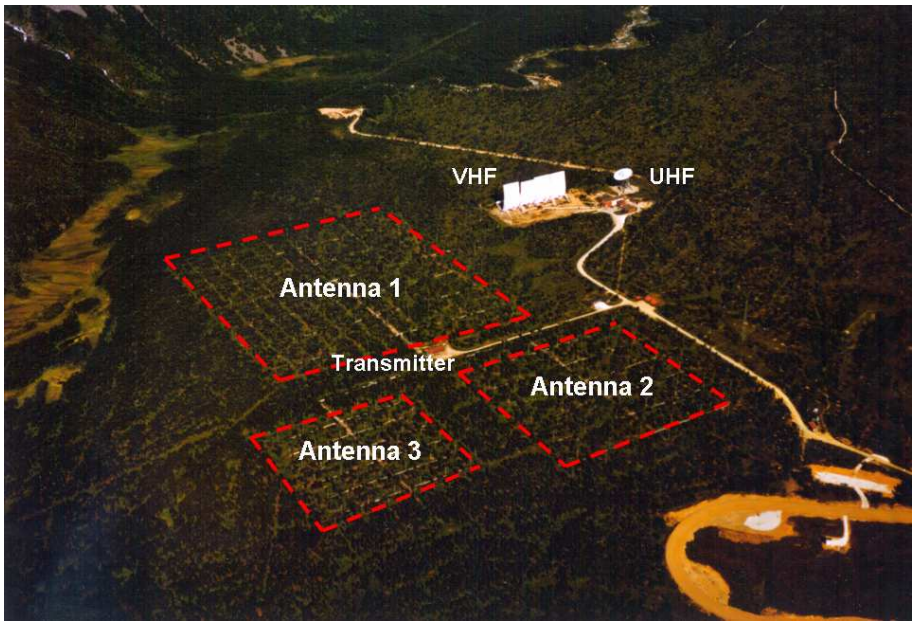

Figure 2.1: The EISCAT site at Tromsø.

2.2 IRIS riometer

Riometer (Relative Ionospheric Opacity Meter using Extra Terrestrial Electromagnetic Radiation) measures the intensity of the radio noise originating from stars or galaxies for monitoring the total column absorption of the radio waves on their way through the ionosphere. By this method, relative changes in the absorption are obtained by comparing the measured radio noise power to a so-called quiet day curve, which represents the power of the radio noise in quiet conditions. One single antenna element enables measuring average absorption integrated practically over the whole sky, whereas imaging riometers (IRIS) use phased arrays to form a number of narrow beams to monitor cosmic radio noise from many directions separately.

The Kilpisjärvi IRIS imaging riometer (Fig. 2.2) in northern Finland (69.05° N, 20.79° E) is supervised by Lancaster University (UK) and operated in conjunction with Sodankylä Geophysical Observatory (SGO). It has been in operation since 2nd September 1994. The system operates at 38.2 MHz and produces an array of 49 narrow beams with widths between 13° and 16°. The phasing of the array is achieved using an assembly of Butler matrices. The basic scanning interval of the array is one second. For further technical details see Detrick and Rosenberg [1990].

Serendipitously, one of the IRIS beams (number 9) overlaps with the vertical EISCAT Heating beam in the D-region. This made it possible to quantify the heating effect on the cosmic radio noise absorption in Paper II by comparing IRIS data measured during periods of heating with subsequent non-heated times.

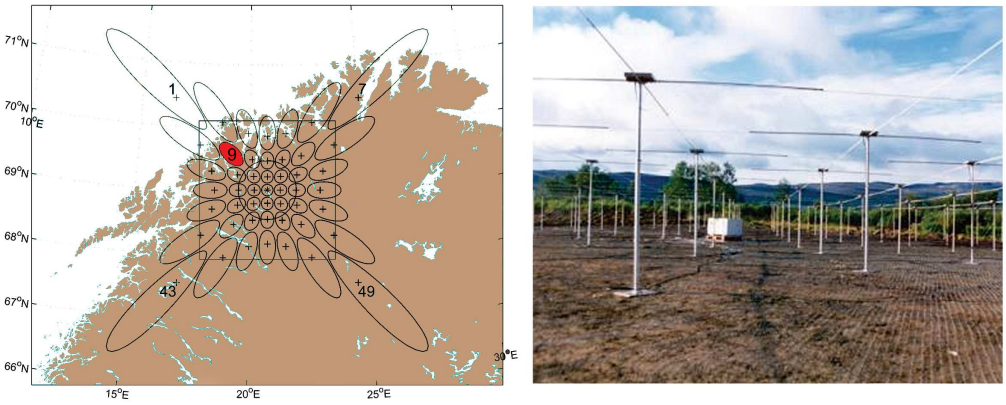

Figure 2.2: Kilpisjärvi IRIS 3 dB beam projections above northern Scandinavia. The highlighted beam number 9 intersects with the vertical EISCAT Heating beam in the D region. (Figures are used with permission of Steve Marple, Department of Communications Systems, Lancaster University.)

Chapter 3

Modelling

3.1 D-region ionosphere as a research target

The D-region ionosphere can be considered as a complex transition region from the collision dominated neutral atmosphere to the ionosphere characterised by plasma features. Especially, modelling of the D region ion chemistry is complicated due to the fact that minor constituents participate significantly in the photochemistry of ions. In addition to molecular ions, such as O_2^+ and NO^+ which are first produced, a multitude of other kinds of ions exists with significant concentrations, such as water cluster ions as well as negative ions [Verronen, 2001]. For the heating diagnostics, the response of the D-region ion chemistry to the varying electron temperature is discussed in the following Section 3.2.

The D-region ionosphere is ionised by solar electromagnetic radiation, energetic particle precipitation and galactic cosmic rays [i.e. Hargreaves, 1992, pp. 229-231]. At daytime, the solar Lyman-α radiation ionises nitric oxide (NO) and EUV affects $O_2(^1\Delta_g)$. At altitudes below 60 km, the main quiet time ionisation source is galactic cosmic ray precipitation. These radiation sources produce quiet-time ionisation rates from 10^4 to 10^7 m^{-3} s^{-1} at D-region altitudes [i.e. Brasseur and Solomon, 2005, pp. 552–553]. However, sporadic ionisation events, such as X-ray bursts from solar flares, relativistic electron precipitation from the radiation belts (affecting mid-latitudes), energetic auroral precipitation (at high latitudes) or solar proton events can increase the ionisation level, and the electron density, by several orders of magnitude.

In general, there are two possible approaches available to observe any atmospheric or ionospheric parameters in the D region. The first option is obviously in-situ measurements, which are limited to rocket-borne instruments in this case. Therefore the current knowledge on D-region composition is founded to a large extend on past rocket missions [e.g. Friedrich et al., 2004]. Besides the cost, sparse spatial and temporal coverage of the data is obviously the drawback of this approach.

Another option is to exploit electromagnetic (or even infrasonic) waves for atmospheric remote sensing. As described already in Chapter 2, the D-region ionosphere is accessed here by remote sensing methods based on radio wave absorption and scattering in the collisional D-region plasma. Firstly, the electron gas is heated by powerful

HF radio waves, and secondly, the effects are monitored by means of incoherent scattering (VHF) and cosmic radio noise monitoring (IRIS).

In general, remote sensing methods need a sufficient amount of a priori information about the target for meaningful interpretation of the data. The SIC model is used for this purpose.

3.2 Sodankylä Ion Chemistry model (SIC)

The Sodankylä Ion Chemistry (SIC) model is a detailed 1-dimensional time-dependent chemistry model, which includes 36 positive ions, 27 negative ions and 14 minor neutrals coupled together via more than 400 reactions [Verronen, 2006]. The model uses the neutral temperature and major atmospheric species as a static background from the empirical MSISE-90 model [Hedin, 1991] and from Shimazaki [1984].

Despite of some critical limitations, such as not-modelled horizontal transportation and energetics, the SIC model has been applied successfully to a variety of applications, including solar proton events affecting odd nitrogen, hydrogen and oxygen [Verronen et al., 2005], sunset transition in the D region [Verronen et al., 2006], ionisation by solar X-ray flares [Enell et al., 2008b] and chemical effect of sprites [Enell et al., 2008a].

In Papers I, III and IV, the SIC model was applied to the diagnostics of heating experiments in different stages. Firstly the model was preconditioned to match the ionosonde-calibrated backscattered power measured by the VHF radar (see Fig. 3.1). This was done by introducing a set of parameterised electron precipitations fluxes as ionisation sources, in addition to solar radiation by Tobiska et al. [2000].

Secondly, the modelled background electron density profile was an input parameter for the radio wave propagation model presented in Section 3.3. Thirdly, the theoretical ACF was calculated based on the SIC-modelled ion composition.

Moreover, in Papers III and IV, SIC model version 7.2, developed as part of the work presented by Enell et al. [2008a], made it possible to set the electron temperature independently from the neutral temperature. This feature was used to parameterise the heating effect on the ion chemistry itself. The chemistry response to the heating, i.e. the relative change of the ion composition as a function of time, was studied for electron temperatures increased by factors of 1.5, 2, 5, 10, 30 and 100 above the neutral temperature. As a result, the chemistry response could be obtained for any given *heating factor*, i.e. electron to neutral temperature ratio, by interpolating between the responses.

As presented in Figure 3.2, the heating effect on the ion chemistry is simulated by increasing the electron temperature by a factor of 5 above the neutral temperature in all altitudes. This "heating on"-period is set to last 6 seconds, and after that the chemistry is let to recover by turning the electron temperature back to the neutral temperature. Hence, the figure shows the characteristic electron density response to transient electron temperature changes in 6 second intervals.

It turns out, that the electron density is decreased during the heating below 70 km due to the increased rate of the electron attachment to neutrals, which produces negative ions. On the other hand, the electron density increases above 80 km due to a decrease in the electron recombination rate.

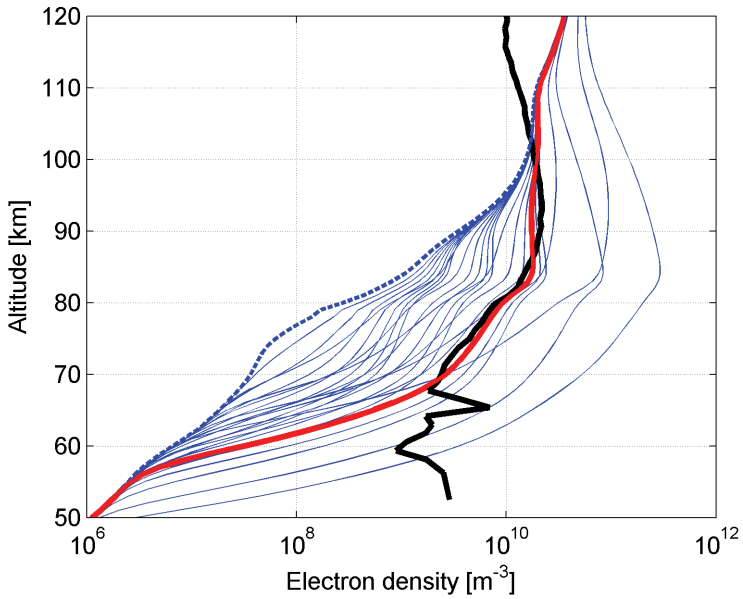

Figure 3.1: SIC modelled electron density profiles for a set of ionisation input parameters (blue) vs. EISCAT VHF measurement on 24 November 2006 09:30 UT (black line). The dashed blue line denotes the electron density profile caused by solar radiation alone [Tobiska et al., 2000]. On top of that, an angularly isotropic Maxwellian electron precipitation with various characteristic energies and fluxes (blue lines) was used to find the best match (red line) to the data.

The analysis of the chemistry response is used in the IS data analysis presented in Paper III. The chemistry turned out to be significant only for the lowest range gates of the VHF radar. However, the electron density modulation driven by negative ion chemistry seems to play a significant role in the Polar Mesosphere Winter Echo modulation as suggested in Paper IV.

3.3 HF radio-wave propagation model

The radio wave propagation in magnetoionic plasma is described by the well-known Appleton theory, which is presented in detail by Budden [1961]. The theory describes the complex refractive indices of the plasma for two polarisations (O- and X-mode) as a function of normalised electron plasma frequency, gyro frequency and electron-neutral collision frequency (see Paper I, Eq. 1). In the original formulation, the effect of electron-neutral collisions was assumed to be independent of the electron velocity. This theory can be generalised for any electron distribution function, especially for Maxwellian, according to Sen and Wyller [1960]. In this thesis, the original Appleton

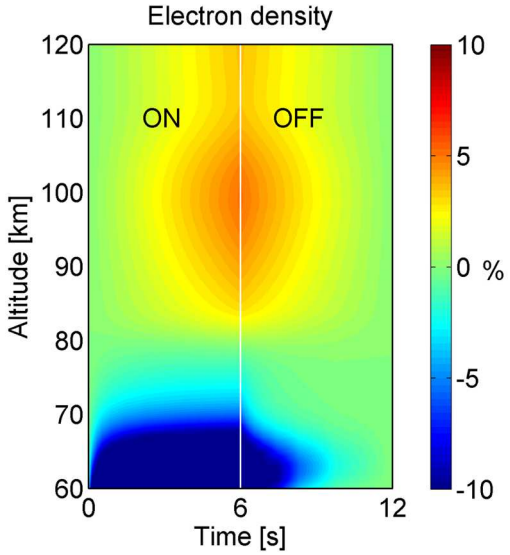

Figure 3.2: SIC modelled electron density response to a 6 second long heater-on period, where the electron temperature is increased by a factor of 5 at all altitudes. After that, the chemistry is allowed to recover in a 6 s long off period by turning the electron temperature back equal to the neutral temperature given by the MSIS-90 model [Hedin, 1991].

formula was used only in Paper I, while in the following Papers II, III and IV, the modelling was done by using the generalised theory.

In presence of collisions between electrons and neutrals, the refractive index of the plasma is a complex number with a negative imaginary part. It describes the absorption of the radio wave intensity given by Eq. 1 in Paper II. The same formulation is used for calculating the absorption of the heater radio wave as well as the cosmic radio noise (Paper II).

The absorbed radio wave energy is transferred into thermal energy of the plasma, or in practise, only to the electron gas due to the huge mass difference between atoms/ions and electrons. The heating-induced electron temperature achieves an equilibrium when the electron energy gain by the radio wave absorption is balanced by the loss processes associated with excitations [Stubbe and Varnum, 1972; Prasad and Furman, 1973; Pavlov, 1998a,b].

Figure 3.3 shows the modelled electron temperature profiles for the EISCAT Heating Antennas 1 and 2 (see Fig. 2.1) emitting O-mode radio waves at their lowest licensed frequencies (5.423 MHz and 4.04 MHz, respectively). In the right panels, the electron temperature is presented along the central line of the heater beam for all of the SIC-modelled electron density profiles shown in Fig. 3.1. The left panels illustrate the heating effect in two dimensions for the electron density profile which matched to the VHF data best.

As a result, the larger Antenna 1 compresses the radiation power into a narrower beam and therefore provides somewhat higher temperatures compared to Antenna 2. Moreover, the heating effect is highly dependent on the electron density profile. In high electron density conditions, the achieved heating effect is generally weaker, and the maximum effect takes place at a lower altitude, compared to lower electron densities. Consistently, the lowest electron density profile marked as a dashed line in Fig. 3.1 corresponds to the highest electron temperature in Fig. 3.3 around 80 km, and vice versa, the highest electron density leads only to a minor effect at 60 km. Naturally, this is caused by strong absorption already at low altitudes in high electron-density conditions.

It is worth mentioning here, that the difference between the results obtained by the original Appleton formula and the generalised expression by Sen and Wyller [1960] can be remarkable. For instance, in case of the modelled heating effect shown in Fig. 3.3 (red line), the original Appleton theory predicts roughly a 40 % smaller heating effect than the generalised calculation.

It is to be noticed also, that an electron density change due to heating (see Fig. 3.2) modifies slightly the opacity of the ionosphere and therefore causes a secondary effect in the heated electron temperature. In practise, this feedback effect to the electron temperature itself turns out to be negligibly small. The small opacity change due to chemistry, however, could be a significant factor in the discrepancy between the modelled heating effect on the cosmic radio noise absorption and the signature found from measurements (Paper II).

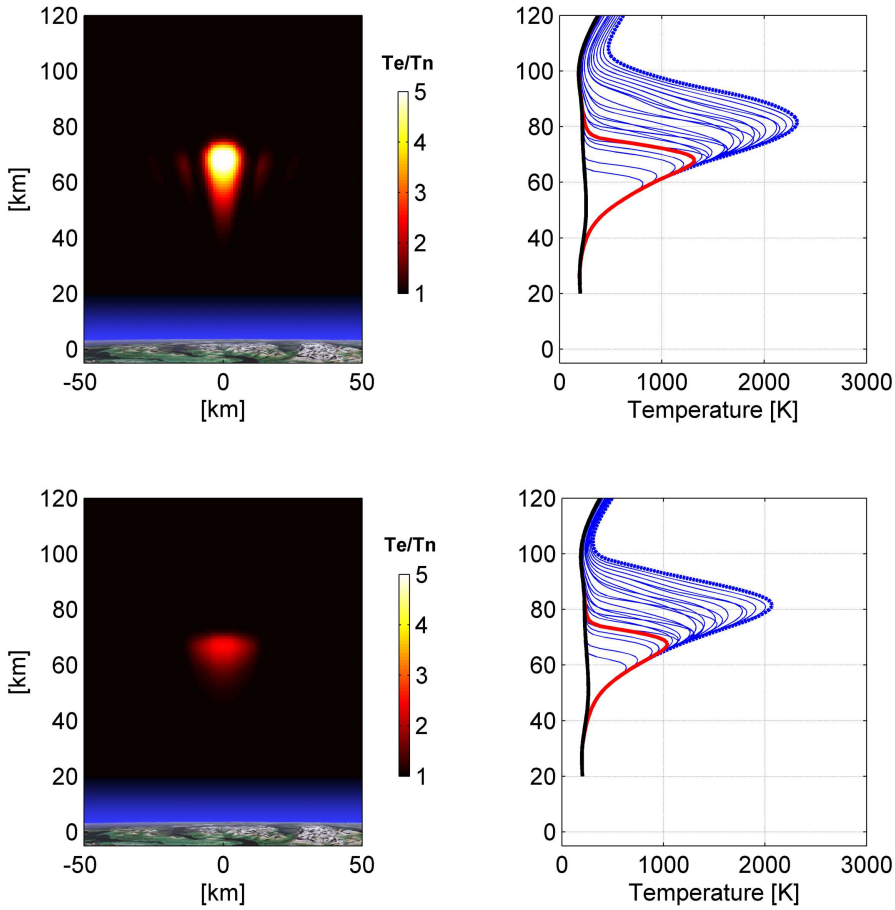

Figure 3.3: Modelled D-region heating effects for the EISCAT Heating Antennas 1 and 2 (upper and lower panels, respectively). Vertical beam, full power, lowest frequency (5.423 MHz for the Antenna 1, 4.04 MHz for the Antenna 2) and O-mode polarisation were used as heater parameters in the model. The modelling represents the conditions during the EISCAT heating experiment on 24 November 2006, 09:30 UT. Panels on the right show the temperature profiles along the centre line of the heater beam for the set of electron density profiles shown in Fig. 3.1. Especially, the modelling for the electron density profile matching the EISCAT data (red line in Fig. 3.1) is marked as red and used in the model runs on the left panels.

3.4 Incoherent scattering from collisional plasma

The incoherent scatter (IS) radar technique is explained in details by Nygren [1996]. In principle, the IS radar transmits a powerful radio wave in order to detect backscattering from thermal fluctuations of the ionospheric plasma. The spectrum of the backscattered signal contains information of the characteristic plasma parameters, such as electron density, electron and ion temperature, and plasma drift velocity.

Although, the Thomson scattering from individual electrons is the microscopic mechanism responsible for the incoherent scatter, the spectrum of the backscattered signal is characterised by two wave modes present at the ionospheric plasma, i.e. ion acoustic and Langmuir waves. Hence, the IS spectrum consists of two ion acoustic components broadened to merge together into a so-called *ion line* and two *plasma lines* due to Langmuir waves. Theoretical IS spectra according to Dougherty and Farley [1960] are presented in the upper panel of Figure 3.4 for different altitudes in the lower ionosphere. These calculations are based on the SIC model results for the heating experiment on 24 November 2006 (Paper III, Case 1).

A hint of the characteristic "double-humped" shape of the ion line is visible in the spectrum corresponding to 120 km (blue lines). Below that, an increasing collision rate between ions and neutrals causes a strong Landau damping of ion acoustic waves, and hence, form the ion line into a narrow, approximately Lorentzian shaped line (red lines).

The plasma lines are located symmetrically on both sides of the radar carrier frequency at a distance equal to the plasma frequency. At the lower D-region altitudes, the distinct plasma lines merge towards the ion line into a continuum of spectral density.

The plasma autocorrelation function, defined as an Inverse Fourier Transform of the IS power spectral density, is shown in the lower panel of Fig. 3.4. However, the ACF detected by the radar is a product of the plasma ACF and so-called *radar ambiguity function* describing the receiver impulse response and the modulation used in the transmission. In Paper I, the effect of ambiguity function is taken into account according to Pollari et al. [1989], while in Papers III and IV, the statistical inversion based data analysis provides directly the estimates of the plasma ACF for a certain bandwidth.

The total backscattered power, given by an integral over the power spectral density, corresponds to the autocorrelation function at zero lag. Because the power depends mainly on the electron content of the target plasma, the background ACF values at zero lag increase monotonically with height.

The heating effect is simulated in Figure 3.4 by increasing the electron temperature by a factor of two above the ion temperature (dashed lines). The electron temperature enhancement spreads the spectral density of the ion line into higher frequencies, and therefore, reduces the power in a band limited to the ion line. Consequently, the heating effect is clearly visible in reduced magnitude of ACF, especially near the zero-lag.

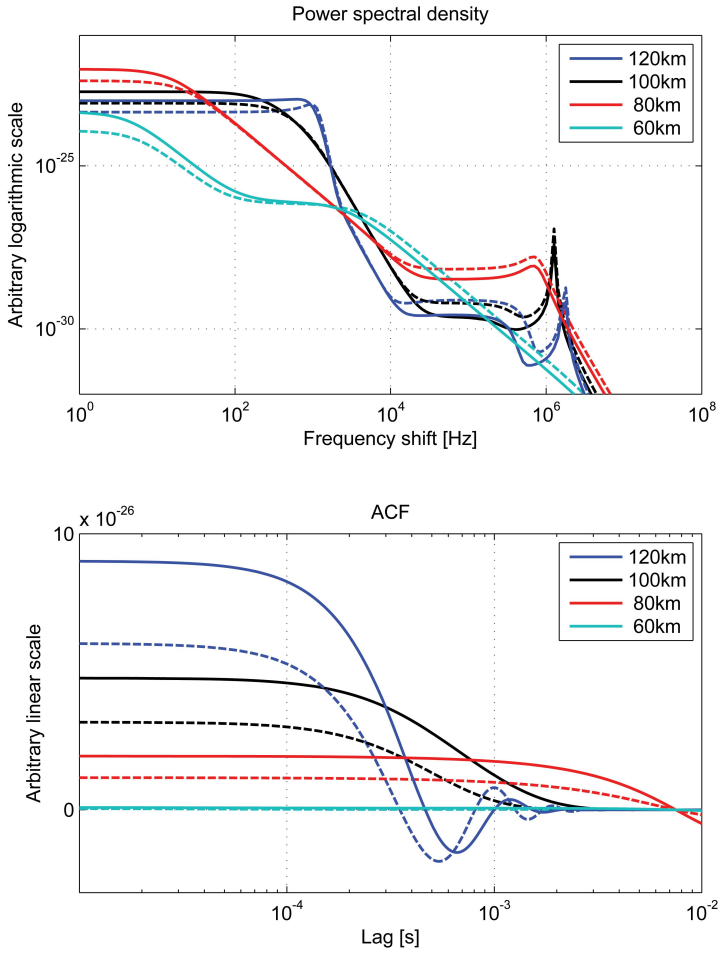

Figure 3.4: Upper panel: Theoretical incoherent scatter spectrum as a function of a positive frequency shift with respect to the EISCAT VHF frequency (224 MHz). Spectra for altitudes of 60, 80, 100 and 120 km are separeted by colours. The ion composition used in the spectrum calculation according to Dougherty and Farley [1963] is based on the SIC model results for the heating experiment on 24 November 2006 (Paper III, Case 1). Solid lines represent the background conditions where electron and ion temperatures are set to the neutral temperature. Dashed lines denote calculations for electron temperatures increased by a factor of 2 above the neutral temperature. Lower panel: Corresponding autocorrelation functions are obtained as an Inverse Fourier Transform of the ion line part of the power spectral density, i.e. 0-250 kHz. These frequency limits represent roughly the bandwidth of the experiment used in Paper III.

Chapter 4

Results

Credibility of modelling is based on experimental verification. Up to the first published incoherent scatter measurements of the heated electron temperature in the D-region ionosphere (Papers I and III), the verification was based alone on indirect evidence, such as successful modelling of ULF-VLF wave generation experiments [Barr, 1998] or modulation of cosmic radio noise absorption (Paper II). Despite the low SNR, IS measurements of the heated D-region ionosphere have become possible by using novel radar techniques, at least in relatively high electron density conditions. These measurements, combined with detailed chemistry modelling, provide new insights into IS radar meausrements and heating experiments, which so far have been concentrated only on the coherent echoes (PMSE, PMWE and API). Paper IV suggests that the negative ion chemistry plays an important role in PMWE modulation along the heater on/off-cycle.

4.1 First IS observation of the D-region heating effect

The HF radio wave propagation model introduced in Section 3.3 was originally developed for the wave generation experiments at the ULF frequency range [Bösinger et al., 2000]. Especially, the model was designed to find an optimal set of heater parameters in different geophysical conditions.

By using this model, we made two surprising discoveries. Firstly, with all reasonable electron density profiles used, the maximum heating effect took place in low D-region altitudes, similarly to those shown in Figure 3.3, instead of in the lower E region where the ionospheric electrojet current flows. Secondly, despite of more than 15 years of EISCAT heating experiments next to the IS radars, we could not find any reports on IS measurements of the D-region heating effect. Since the EISCAT Heating should be capable of increasing the electron temperature, according to the model, by a factor of 10 or even more in some conditions, we decided to investigate this issue.

A successful experiment was carried out on 19 November 1998 from 20.30 UT until midnight. The heater parameters were chosen to maximise the effect according to the

model. A vertical radio wave beam was generated by the largest EISCAT Heating Antenna array 1. The lowest possible frequency 5.423 MHz and X-mode polarisation were chosen to maximise the absorption, and hence, the effect. The heater operated in a simple 5 minutes on/off modulation scheme.

In the analysis, the autocorrelation functions measured by the VHF radar were integrated over the whole experiment time separately for the heater on and off periods. After that, a special ambiguity correction by Pollari et al. [1989] was applied to the data in order to separate the measurement device ambiguity function from the plasma ACF. The ambiguity corrected ACFs are shown in Fig. 2 of the Paper I. There is a clear difference in the data between the heater on and off periods in all of the range gates shown, starting from 78 km. The electron-to-ion temperature ratio was used as a free parameter in fitting a theoretical ACF to the data as shown in Fig. 4.1.

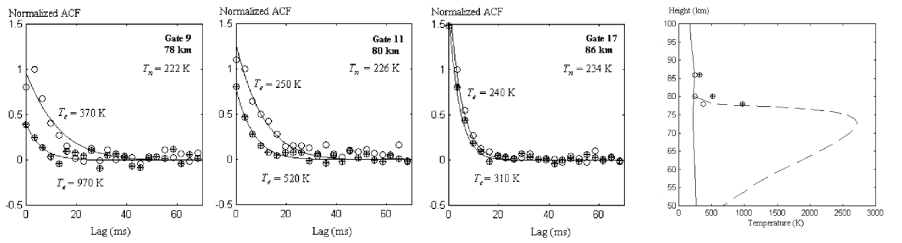

Figure 4.1: Summary of the results of Paper I. The three leftmost panels show the fitting of the IS theory [Dougherty and Farley, 1963] to the ambiguity corrected ACFs, separately for the heater on and off periods (open and crossed circles, repectively). The neutral temperature, which is assumed to be equal to the ion temperature, is taken from the MSISE-90 model [Hedin, 1991]. The electron temperature is estimated by using the electron to ion temperature ratio as a free parameter in the fitting. The results are compared to the theoretical heating model in the leftmost panel. For more details, see Paper I.

As a result, the electron temperatures were estimated successfully at a few altitudes on the upper edge of the expected heating effect. These electron temperature estimates fit reasonably well to the modelled temperature profile. Unfortunately, the data were too noisy for the analysis at the altitudes of the expected maximum effect. This paper demonstrated, however, that the heating effect can be detected by IS techniques in the D-region ionosphere during suitable conditions. Based on the results shown in Papers I and III, the optimal electron density profile in this application should be high enough for a sufficient SNR of the IS signal, but still not too high causing too

much absorption below the detection altitude.

4.2 Modulation of the cosmic radio noise absorption

After the first successful measurement of the electron temperature in the heated D region (Paper I), the experiment was repeated several times but without success. The reason for the failures was simply an insufficient SNR due to low electron density during the experiments.

After a few years in different projects, we reconsidered the problem of verifying the D-region heating effect, but this time using the cosmic radio noise absorption as an indicator. This method was earlier suggested by Pashin et al. [2003]. In their theoretical paper, the cosmic radio noise absorption at 38.2 MHz was estimated to increase due to heating by 0.2–0.5 dB, which should be easily detectable by the riometer technique. We confirmed these theoretical estimates by using the SIC model by Enell et al. [2005]. Two reasons was presented for the expected change of the D-region opacity. Primarily, the heating of the electron gas leads to higher collision rate between electrons and neutrals, and hence, to a stronger absorption of radio waves. This effect takes place within a few milliseconds. Secondarily, the absorption was expected to change due to electron-temperature dependent ion chemistry.

Probably by a fortunate co-incidence, one of the 49 beams of the Kilpisjärvi IRIS riometer overlaps with the vertical EISCAT Heating beam at D-region altitudes. This makes it possible to calculate the difference between the cosmic radio noise absorption during the heater on and the subsequent heater off periods. We conducted a statistical survey of this so-called *absorption difference* through all suitable heating experiments since the start of IRIS operations (1994–2004). The median value of the absorption difference for all of the 49 IRIS beams is shown in Fig. 4.2.

Instead of the expected magnitude of the D-region absorption difference, which should be easily distinguished within individual heater on/off modulations, the median absorption increase in the overlapping beam 9 was found to be of the order of 0.003 dB. This extremely faint signature was, however, statistically significant according to the bootstrap error analysis [Efron, 1979]. Moreover, the effect is clear when compared to all the other 48 IRIS beams pointing in different directions.

This was the first experimental result showing the heating-induced change in D-region opacity for cosmic radio noise, while the heater generated scintillations in F-region altitudes were observed for several times [e.g. Basu et al., 1987; Costa et al., 1997; Honary et al., 2000].

In previous theoretical works [Enell et al., 2005; Pashin et al., 2003], the geometry of the overlapping heater and riometer beams was oversimplified, which could partly explain the discrepancy between the theoretical estimates and observations. In Paper II, a detailed modelling of the cosmic radio noise absorption along 401 rays through the ionosphere was introduced. The heating effect was calculated in 1-km steps along each ray taking into account the actual directional patterns of the EISCAT Heating antennas. The total absorption measured by the IRIS beam 9 was estimated as a directional pattern weighted mean of the absorption values. The absorption difference between heated and background ionospheres was calculated for EISCAT Heating

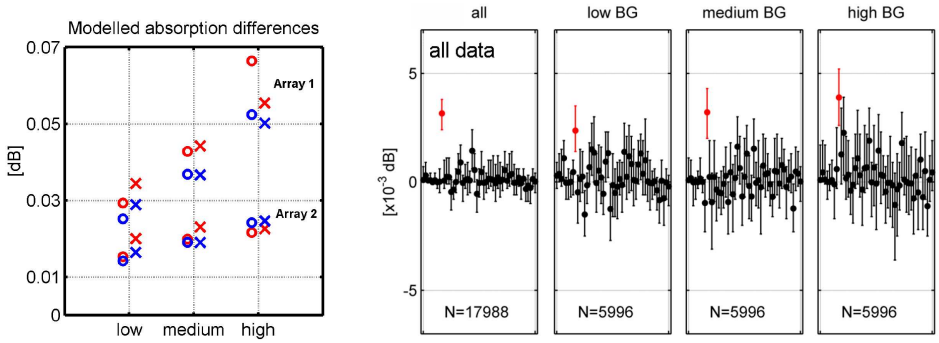

Figure 4.2: Summary of Paper II. Left panel: Theoretical cosmic radio noise absorption differences between the heater on and off periods for the IRIS riometer (32.8 MHz) beam number 9 in low, medium and high electron density conditions. The results are shown for the EISCAT Heating Antennas 1 and 2, for both modes (o,x) and for winter and summer atmospheres (blue and red, respectively). Four panels on the right: Medians of the observed absorption differences, with 95% significance levels, for all 49 IRIS beams. The overlapping beam number 9 is shown in red.

Antennas 1 and 2, for three electron density profiles (low, medium and high), for both modes (o and x), and for summer and winter neutral atmospheres. These results are summarised in the left panel of Figure 4.2.

It turned out, that a proper treatment of the geometry reduces the absorption difference estimates by an order of magnitude as compared to the idealised assumptions of perfectly overlapping and uniform beams. However, a remarkable difference between the data and the model remains. Interestingly, despite the quantitative discrepancy, there are eye-catching similarities between the model and the data. Firstly, the statistical effect grows monotonically as a function of background absorption, which can be regarded as a measure of the electron content in the D region. Similarly, the model predicts systematically stronger effects for profiles of high electron density (see Fig. 4.2). Secondly, the more intense heater beam generated by Antenna 1 seems to cause approximately a twice as strong effect as Antenna 2. This is visible both in the data (Paper II, Fig. 8) and the model (Fig. 4.2).

In addition to statistical uncertainty analysis of the data, several robustness tests were carried out also for the modelling (see Paper II, Fig. 5). It turned out, that any reasonable variance in the actual direction of the IRIS beam or in the heater frequency could not explain the overestimates of the absorption effect.

This discrepancy still remains an open question. In Paper II, we speculate about the possibility that the actual electron temperature achieved in heating experiments is significantly overestimated in the present model, either due to an overestimated absorption, or some unknown electron energy loss process. At the moment of writing Paper II, the chemistry effects were erroneously ruled out based on results of Enell et al. [2005], where they seemed to cause only minor changes over relatively long timescales. On the other hand, the chemistry effect on the heating itself was tested and found to be negligibly small. However, Papers III and IV indicated that the heating effect on the negative ion chemistry should have been taken into account.

Obtaining a representative estimate for the heater-induced chemistry impact on cosmic radio noise absorption is not a trivial problem, since the characteristic response of the electron density (Fig. 3.2) depends on the background conditions of the ionosphere. It is to be noted that the SIC model was not used at all in Paper II, instead, the characteristic electron profiles (low, medium, high) were taken from rocket measurements [Friedrich et al., 2004]. By this choice we wanted to make the theoretical estimates independent of another theoretical tool.

In order to demonstrate the possible importance of a change in chemistry, the same parameterised electron density response to the heating as shown in Fig. 3.2 was used in the re-calculation of the theoretical absorption differences, shown in Fig. 4.3.

First of all, the chemistry makes a significant difference to the estimates. In the cases of "low" and "medium" electron density profiles, the chemistry parameterisation decreases the absorption difference estimates to the same order of magnitude as the values found in the data. In the high electron density cases, on the other hand, taking the chemistry effect into account makes the model results even more overestimated as compared to the actual data. As a conclusion, a small change in the ion chemistry due to heating, which may be negligible in some applications, may offer an explanation for the large *relative*, but small *absolute* difference between the model and observations. However, these must be regarded as preliminary considerations, since the chemistry

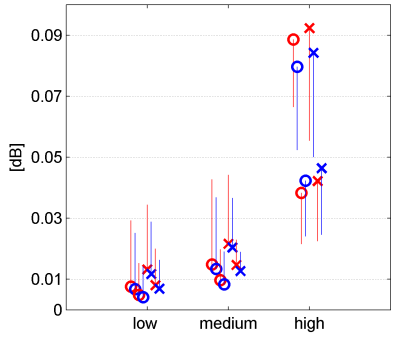

Figure 4.3: Estimated change of the theoretical absorption difference due to chemistry. The markers denote the new values and the lines point at the original results calculated using a constant electron density (see Fig. 4.2).

parameterisation used may not represent the electron density response well under different geophysical conditions.

4.3 New IS methods utilised

Almost a decade after the first IS observation of the electron temperature in the heated D-region ionosphere (Paper I), the experiment was repeated as an updated version in the Finnish EISCAT campaign of November 2006. In recent years, there has been a strong development of the IS radar technique by the Inverse Problems group at SGO.

The traditional IS technique determines the ACF estimates by a hardware correlator. Nowadays, this can be replaced by direct sampling of the transmitted and received signals. As a results, the ACF estimates are calculated from the raw data by means of statistical inversion. These D-region heating experiments were one of the first scientific applications where the new methods were successfully exploited.

For the heater operation, we adopted again a straightforward approach. EISCAT Heating Antenna 1 was used to form a vertical beam providing maximum radiation power available, which is approximately 600 MW ERP at 5.423 MHz. The heater was modulated repeatedly with a simple pattern (O-mode/off/X-mode/off) in 6 s intervals.

Figure 1 in Paper III shows the VHF data for the six cases studied. The differences of the integrated ACFs between the heater on and off periods are re-plotted in Fig. 4.4 showing in addition the modelled heating factors. There is a clear signa-

ture of heating visible in the data, i.e. a reduction of the magnitude of the ACF in the heated ionosphere. Moreover, the altitude of this signature varies from case to case, depending on the prevailing conditions. Also the modelled heating effect follows roughly the altitude of the signature.

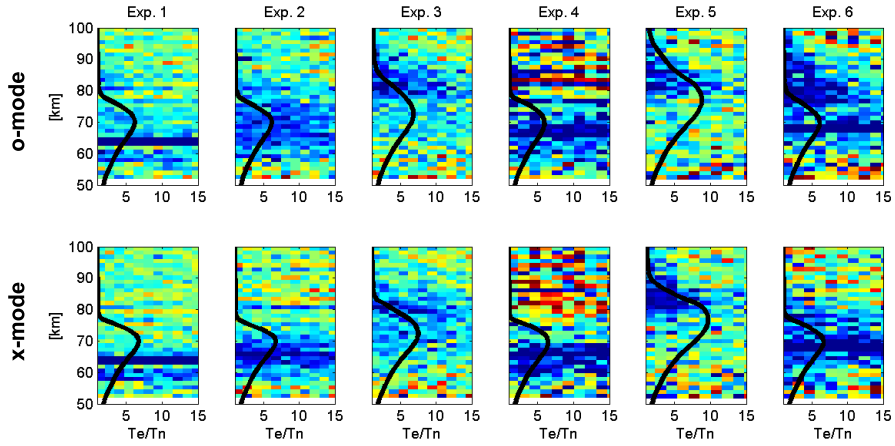

Figure 4.4: Modelled heating effect for the six cases studied in Paper III (black lines) for both modes. The difference between the mean ACF during the heater on and off periods are shown on the background in arbitrary color scale (see the two lowermost panels of Fig. 1 in Paper III).

The electron temperature estimates were obtained from the ACFs by fitting an exponential ACF [Fukuyama and Kofman, 1980] to the data with the Markov Chain Monte Carlo (MCMC) method [Hastings, 1970]. The usage of the SIC model in the analysis was twofold. Firstly, the prior probability distributions of the fitted plasma parameters were selected according to the SIC profiles and secondly, the ion chemistry response to the heating was parameterised for each of the cases. Details of the analysis are described in Section 3 of Paper III.

As a result, the MCMC method gives a posteriori probability distribution of the fitted plasma parameters. Fig. 4.5 shows these distributions for the electron temperature in the cases 1, 2 and 4, where it was possible to estimate the electron temperature at the altitudes of the predicted maximum heating within a reasonable accuracy. These are the first successful IS measurements in the altitudes of the expected electron temperature maximum.

There was a fairly good agreement between the theoretical heating model and the data in cases 2 and 4 at the altitudes of the maximum effect. On the other hand, an unexpectedly weak effect was found in case 1. In the discussion of Paper III, we

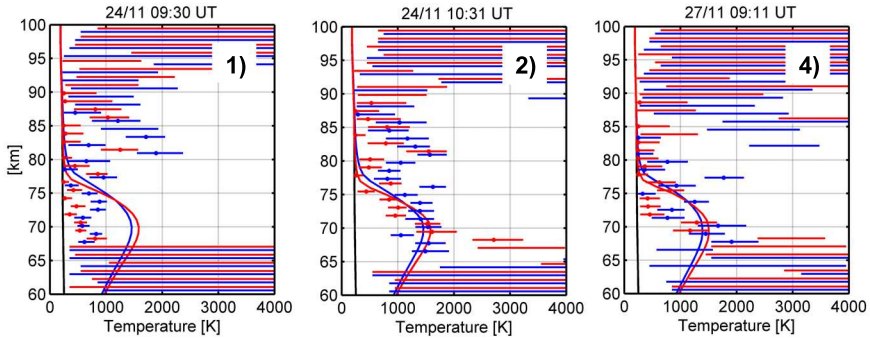

Figure 4.5: The main result of Paper III: first electron temperature measurements at the altitudes of the maximum effect in the heated D-region ionosphere compared to the model results (blue, red and black denote O-mode, X-mode and off period, respectively). Error bars represent 90% significance levels according to the MCMC analysis described in Chapter 3.3 of Paper III. The most probable temperatures are shown as dots whose uncertainty is less than a threshold value of 1000 K. The solid curves represent the modelled temperatures.

state that this might be associated with a strong PMWE at 64 km altitude, since the electron temperature was found to be consistent with the model in the Case 2, which represents approximately the same ionospheric conditions one hour later, but without PMWE (see Fig. 4.4).

4.4 PMWE modulation

Previously, in Paper III, the ion-chemistry response to the heating was parameterised according to the SIC model. Our original idea was to investigate if it is possible to see signatures of the chemistry in the IS signal. Although the chemistry caused only minor changes in the electron temperature estimates, limited to the altitudes of the heating maximum and below, the timescales of negative ion chemistry changes matched to the variation of the PMWE power in Case 1. The heating-induced modulation of PMWE was just recently discovered [Kavanagh et al., 2006; Belova et al., 2007] and its cause was unknown.

The Super-imposed Epoch Analysis (SEA) shown in Fig. 4.6 reveals the characteristic PMWE response to the heating. The distributions of the individual SEA estimates are presented in vertical grayscale histograms along the 6 second on/off heating cycle. In addition, the error bars show the limits of 50% centermost points in the distributions.

The analysis shows that the PMWE power is reduced approximately to half of the background level after the heater is turned on, and when turned off, the echo power recovers to the original level. Both these transitions take approximately two seconds. This timescale matches the characteristic recovery time of the disturbed negative ion chemistry observed in the API experiments by Rietveld et al. [e.g. 1996].

As a first order approximation, the PMWE power is proportional to the electron density squared [Lübken et al., 2006]. Under this assumption, the modelled response of PMWE, i.e. the relative change of N_e^2, is compared to the observed PMWE modulation in Fig. 4.6. The curves correspond to the electron to neutral temperature ratios of 5, 10 and 30 during the heater on period. The comparison shows that the electron-temperature dependent electron-density modulation can explain both the magnitude and the timescale of the characteristic PMWE modulation. However, the assumption of PMWE being proportional to electron density squared may be oversimplified, since it is derived for a stationary situation (see Discussion of Paper IV). Nevertheless, this work suggests that the electron density modulation plays an important role in the PMWE modulation.

Figure 4.7 illustrates the chemical reactions behind the electron density reduction due to heating (red lines). The primary negative ion O_2^- is produced via the electron temperature dependent attachment process. The following reactions in the chain transfer O_2^- ions effectively into CO_4^- and CO_3^-. In the end of the heating period only 32% of the electron density decrease is due to O_2^-, while CO_4^- and CO_3^- correspond to 22% and 46%, respectively. The loss reaction chain (blue lines) leads to saturation during the heater-on period, and recovery when the heater is turned off. Since the chemical reaction rates depend on the concentrations of the reactants, the characteristic PMWE modulation may provide a tool for remote sensing of these constituents

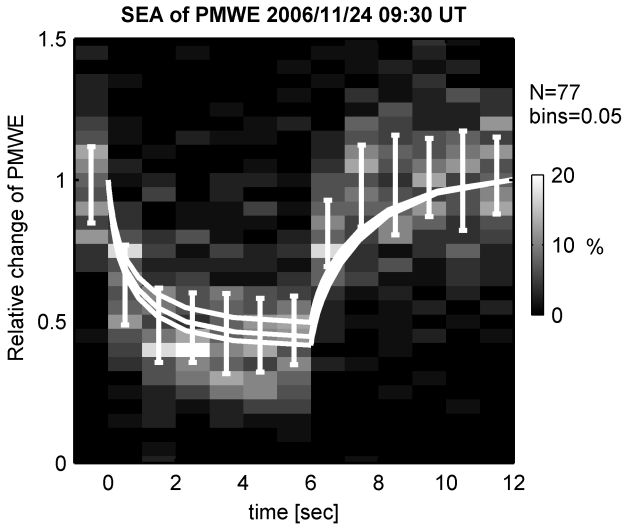

Figure 4.6: The main result of Paper IV: Superimposed Epoch Analysis (SEA) of the PMWE strength and SIC modeled change of N_e^2. The distributions of the superimposed PMWE power estimates are illustrated as vertical grayscale histograms. The error bars represent the limits of the 50% centermost SEA estimates. The solid lines show the SIC modeled N_e^2 response to the 6 second on/off heating corresponding to electron-neutral temperature ratios of 5 (upper line), 10 (middle) and 30 (lower) during the on period.

in the mesosphere. For this, however, an established theory of the PMWE and its modulation is needed.

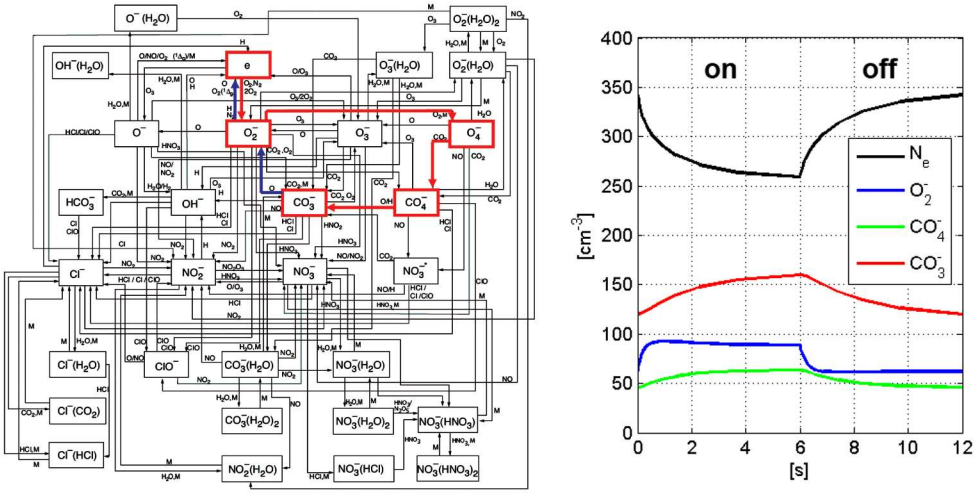

Figure 4.7: Left: The whole negative ion chemistry scheme of the SIC 7.2 model is illustrated as a flow chart (black lines). The most prominent reaction chain causing the electron-density reduction during the heater-on period is marked as red arrows. Blue arrows denote the main reaction chain causing the negative ion loss. Right: Time evolution of the most important negative ion concentrations causing the electron-density modulation.

Chapter 5

Concluding remarks

In near future, the current EISCAT IS radars will be replaced by a new radar system consisting of multiple phased array antennas in northern Scandinavia and therefore providing a 3D view of the ionosphere at high latitudes. The EISCAT Heating will also be upgraded making it possible to design new heating experiments. These next generation EISCAT facilities will be key instruments in the research of the solar impact on the polar upper atmosphere.

This thesis demonstrates the potential of the active heating technique in D-region ionosphere research, a method which is far from fully utilised at the moment. First of all, the electron temperature in the D-region ionosphere during the heating experiment is finally measured by the EISCAT VHF radar. The results are found to be in a reasonable agreement with theoretical models. Also the heating-induced reduction of the cosmic radio noise flux, propagating through the heated volume in the D-region altitudes, is detected for the first time. Surprisingly, the effect turns out to be extremely faint, which contradicts the model predictions.

The heating effect on the daytime ion chemistry in the D region is investigated by means of the SIC model. In the cases studied, the chemistry change is limited to the altitudes of the maximum electron temperature. There, the heating strengthens the electron attachment to neutrals producing an increased amount of negative ions. Although this effect contributes to the IS results only in scales of measurement uncertainties, it offers a potential explanation for the PMWE modulation. Moreover, the discrepancy between the modelled and the observed heating effect on the cosmic radio noise absorption could possibly be explained by the chemistry.

Bibliography

Bailey, V. A. and Martyn, D. F.: Interaction of radio waves, Nature, 133, 218, 1934.

Balsley, B. B., Ecklund, W. L., and Fritts, D. C.: VHF echoes from the high-latitude mesosphere and lower thermosphere, observations and interpretations, J. Atm. Sci., 40, 2451–2466, 1983.

Barr, R.: The generation of ELF and VLF radio waves in the ionosphere using powerful HF transmitters, Adv. Space Res., 21, 677–687, 1998.

Basu, S., Stubbe, P., Kopka, H., and Waaramaa, J.: Daytime scintillations induced by high-power HF waves at Tromsø, Norway, J. Geophys. Res., 92, 11 149–11 157, 1987.

Belikovich, V. V., Benediktov, E. A., Tolmacheva, A. V., and Bakhmet'eva, N. V.: Ionospheric Research by Means of Artificial Periodic Irregularities, Copernicus GmbH, Katlenburg-Lindau, Germany, English edn., 2002.

Belova, E., Chilson, P. B., Kirkwood, S., and Rietveld, M. T.: The response time of ionospheric heating to PMSE, J. Geophys. Res., 108, 8446–+, doi: 10.1029/2002JD002385, 2003.

Belova, E., Smirnova, M., T., R. M., Isham, B., Kirkwood, S., and Sergienko, T.: First Observation of the overshoot effect for polar mesosphere winter echoes during radiowave electron temperature modulation, Geophys. Res. Lett., 35, L03 110, 2007.

Bösinger, T., Pashin, T., Kero, A., Pollari, P., Belyaev, P., Rietveld, M., Turunen, T., and Kangas, J.: Generation of artificial magnetic pulsations in the Pc 1 frequency range by periodic heating of the Earth's ionosphere: indications of ionospheric Alfvén resonator effects, J. Atmos. Sol.-Terr. Phys., 62, 277–297, 2000.

Brändström, B. U. E., Leyser, T. B., Steen, Å., Rietveld, M. T., Gustavsson, B., Aso, T., and Ejiri, M.: Unambiguous evidence of HF pump-enhanced airglow at auroral latitudes, Geophys. Res. Lett., 26, 3561–3564, 1999.

Brasseur, G. P. and Solomon, S.: Aeronomy of the Middle Atmosphere, Springer Verlag, The Netherlands, 2005.

Budden, K. G.: Radio waves in the ionosphere, Cambridge University Press, London, UK, 1961.

Chen, C. and Scales, W. A.: Electron temperature enhancement effects on plasma irregularities associated with charged dust in the Earth's mesosphere, J. Geophys. Res., 110, A12 313, 2005.

Chilson, P. B., Belova, E., Rietveld, M. T., Kirkwood, S., and Hoppe, U.-P.: First artificially induced modulation of PMSE using the EISCAT heating facility, Geophys. Res. Lett., 27, 3801–3804, 2000.

Costa, E., Basu, S., Livingston, R. C., and Stubbe, P.: Multiple baseline measurements of ionospheric scintillation induced by high-power HF waves, Radio Sci., 32, 191–197, 1997.

Czechowsky, P., Reid, I., Rüster, I. M., and Shmidt, G.: VHF radar echoes observed in the summer and winter polar mesosphere over Andøya, Norway, J. Geophys. Res., 94, 5199–5217, 1989.

Detrick, D. L. and Rosenberg, T. J.: A Phased-Array Radiowave Imager for Studies of Cosmic Noise Absorption, Radio Sci., 25, 325–338, 1990.

Dougherty, J. P. and Farley, D. T.: A theory of incoherent scattering of radio waves by a plasma, Proc. Roy. Soc. London, A, 259, 79–99, 1960.

Dougherty, J. P. and Farley, D. T.: A Theory of Incoherent Scattering of Radio Waves by a Plasma: 3. Scattering in a Partly Ionized Gas, J. Geophys. Res., 68, 5473–5486, 1963.

Ecklund, W. L. and Balsley, B. B.: Long-term observations of the arctic mesosphere with the MST radar at Poker Flat, J. Geophys. Res., 86, 7775–7780, 1981.

Efron, B.: Bootstrap Methods. Another Look at the Jackknife., Annals of Statistics, 7, 1–26, 1979.

Enell, C.-. F., Arnone, E., Adachi, T., Chanrion, O., Verronen, P. T., Seppälä, A., Neubert, T., Ulich, T., Turunen, E., Takahashi, Y., and Hsu, R.-R.: Parameterisation of the chemical effect of sprites in the middle atmosphere., Ann. Geophys., 26, 13–27, 2008a.

Enell, C.-. F., Verronen, P. T., Beharrell, M. J., Vierinen, J. P., Kero, A., Seppälä, A., Honary, F., Ulich, T., and Turunen, E.: Case study of the mesospheric and lower thermospheric effects of solar x-ray flares: Coupled ion-neutral modelling and comparison with EISCAT and riometer measurements., Ann. Geophys., 26, 2231–2321, 2008b.

Enell, C.-F., Kero, A., Turunen, E., Ulich, T., Verronen, P. T., Seppälä, A., Marple, S., Honary, F., and Senior, A.: Effects of D-region RF heating studied by the Sodankylä Ion Chemistry model, Ann. Geophys., 23, 1575–1583, 2005.

Folkestad, K., Hagfors, T., and Westerlund, S.: EISCAT: An updated description of technical characteristics and operational capabilities, Radio Sci., 18, 867–879, 1983.

Friedrich, M., Harrich, M., Torkar, K. M., and Kirkwood, S.: The disturbed auroral ionosphere based on EISCAT and rocket data, Adv. Space Res., 33, 949–955, 2004.

Fukuyama, K. and Kofman, W.: Incoherent scattering of an electromagnetic wave in the mesosphere: A theoretical consideration, J. Geomag. Geoelectr., 32, 67–81, 1980.

Gabrielli, P., Barbante, C., Plane, J. M. C., Varga, A., Hong, S., Cozzi, G., Gaspari, V., Planchon, F. A. M., Cairns, W., Ferrari, C., Crutzen, P., Cescon, P., and Boutron, C. F.: Meteoric smoke fallout over the Holocene epoch revealed by iridium and platinum in Greenland ice, Nature, 432, 1011–1014, doi: doi:10.1038/nature03137, 2004.

Getmatsev, G. G., Zuikov, N. A., Kotik, D. S., F., M. L., and A., M. N.: Combination frequencies in the interaction between high-power short-wave radiation and ionospheric plasma, JETP Letters, 20, 101–102, 1974.

Hagfors, T., Kildal, P. S., Kärcher, H. J., Liesenkötter, B., and Schröer, G.: VHF parabolic cylinder antenna for incoherent scatter radar research, Radio Sci., 17, 1607–1621, 1982.

Hargreaves, J.: The solar-terrestrial environment, Cambridge University Press, 1992.

Hastings, W. K.: Monte Carlo Sampling Methods Using Markov Chains and Their Applications, Biometrika, 57, 97–109, JSTOR doi:10.2307/2334940, 1970.

Havnes, O.: Polar mesospheric summer echoes PMSE overshoot effect due to cycling of electron heating, J. Geophys. Res., 109, A02 309, 2004.

Hedin, A. E.: Extension of the MSIS Thermospheric Model into the Middle and Lower Atmosphere, J. Geophys. Res., 96, 1159–1172, 1991.

Honary, F. H., Marple, S., and Kavanagh, A.: Heater-induced Scintillation, in: 20th Anniversary Symposium on Ionospheric Interactions in Tromsø, EISCAT Scientific Association, Ramfjordmoen, Norway, 2000.

IPCC: Climate Change 2007: The Physical Science Basis. Contribution of Working Group I to the Fourth Assessment Report of the Intergovernmental Panel on Climate Change, Cambridge University Press, Cambridge, UK, ISBN 978-0-521-88009-1, 2007.

Karashtin, A. N., Shlyugaev, V. Y., Abramov, V. I., F., B. I., Berezin, I. V., Bychkov, V. V., Eryshev, E. B., and Komrakov, G. P.: First HF radar measurements of summer mesopause echoes at SURA, Ann. Geophys., 15, 935–941, 1997.

Kavanagh, A. J., Honary, F., Rietveld, M. T., and Senior, A.: First observations of the artificial modulation of polar mesospheric winter echoes, Geophys. Res. Lett., 33, L19 801, 2006.

Kirkwood, S., Chilson, P., Belova, E., Dalin, P., Häggström, I., Rietveld, M., and Singer, W.: Infrasound - the cause of strong Polar Mesosphere Winter Echoes?, Ann. Geophys., 24, 475–491, 2006.

Kosch, M. J., Pedersen, T., Rietveld, M., Gustavsson, B., Grach, S. M., and Hagfors, T.: Artificial optical emissions in the high-latitude thermosphere induced by powerful radio waves: An observational review, Adv. Space Res., 40, 365–376, 2007.

Lehtinen, M. S.: On optimatization of incoherent scatter measurements, Adv. Space Res., 9, 133–141, 1989.

Lehtinen, M. S., Virtanen, I. I., and Vierinen, J.: Fast comparison of IS radar code sequences for lag profile inversion, Ann. Geophys., 26, 2291–2301, 2008.

Lopéz-Puertas, M., Funke, B., Gil-Lopéz, S., Clarmann, T. v., Stiller, G. P., and Höpfner, M.: Observation of NOx enhancement and ozone depletion in the northern and southern hemispheres after the October-November 2003 solar proton events, J. Geophys. Res., 110, A09S43, 2005.

Lübken, F.-J., Strelnikov, B., Rapp, M., Singer, W., Latteck, R., Brattli, A., Hoppe, U.-P., and Friedrich, M.: The thermal and dynamical state of the atmosphere during polar mesosphere winter echoes, Atmos. Chem. Phys., 6, 13–24, 2006.

Nygren, T.: Introduction to incoherent scatter measurements, Invers Publications, Invers Oy, P.O. Box 105, FIN-99601 Sodankylä, Finland, ISBN 951-97489-0-3, 1996.

Pashin, A. B., Kotikov, A. L., and Pudovkin, M. I.: Numerical simulation of auroral absorption in the artificially disturbed ionosphere, Geomagnetism and Aeronomy, 43, 59–62, 2003.

Pavlov, A. V.: New electron energy transfer rates for vibrational excitation of N_2, Ann. Geophys., 16, 176–182, 1998a.

Pavlov, A. V.: The role of vibrationally excited oxygen and nitrogen in the ionosphere during the undisturbed and geomagnetic storm period of 6–12 April 1990, Ann. Geophys., 16, 589–601, 1998b.

Pollari, P., Huuskonen, A., Turunen, E., and Turunen, T.: Range ambiguity effects in a phase-coded D-region incoherent scatter radar experiment, J. Atmos. Sol.-Terr. Phys., 51, 937–945, 1989.

Prasad, S. S. and Furman, D. R.: Electron energy tranfer rates in the ionosphere, J. Geophys. Res., 78, 6701–6707, 1973.

Randall, C. E., Rusch, D. W., Bevilacqua, R. M., Hoppel, K. W., and D., L. J.: Polar Ozone and Aerosol Measurement (POAM) II stratospheric NO2, 1993–1996, J. Geophys. Res., 103, 28,361–28,372, 1998.

Rapp, M. and Lübken, F.-J.: Polar mesosphere summer echoes (PMSE), review of observations and current understanding, Atmos. Chem. Phys., 4, 2601–2633, 2004.

Rietveld, M. T., Kohl, H., Kopka, H., and Stubbe, P.: Introduction to ionospheric heating at Tromsø-I. Experimental overview, J. Atmos. Terr. Phys., 55, 577–599, 1992.

Rietveld, M. T., Turunen, E., Matveinen, H., Goncharov, N. P., and Pollari, P.: Artificial periodic irregularities in the auroral ionosphere, Ann. Geophys., 14, 1437–53, 1996.

Rietveld, M. T., Isham, B., Grydeland, T., Hoz, C. L., Leyser, T. B., Honary, F., Ueda, H., Kosch, M., and Hagfors, T.: HF-Pump-Induced Parametric Instabilities in the Auroral E-Region, Adv. Space Res., 29, 1363–1368, 2002.

Röttger, J., LaHoz, C., Kelley, M. C., Hoppe, U.-P., and Hall, C.: The structure and dynamics of polar mesosphere summer echoes observed with the EISCAT 224 MHz radar, Geophys. Res. Lett., 15, 1353–1356, 1988.

Röttger, J., Rietveld, M. T., LaHoz, C., Hall, C., Kelley, M. C., and Swartz, W.: Polar mesosphere summer echoes observed with the EISCAT 933-MHz radar and the CUPRI 46.9MHz radar, their similarity to 224 MHz radar echoes and their relation to turbulence and electron density profiles, Radio Sci., 25, 671–687, 1990.

Rozanov, E., Callis, L., Schlesinger, M., Yang, F., Andronova, N., and Zubov, V.: Atmospheric response to NOy source due to energetic electron precipitation, Geophys. Res. Lett., 32, L14 811, 2005.

Scales, W. A. and Chen, C.: On the initial perturbation of mesospheric dust associated irregularities by high powered radio waves, Adv. Space Res., 41, 50–56, 2008.

Sen, H. K. and Wyller, A. A.: On the Generalization of the Appleton-Hartree Magnetoionic Formulas, J. Geophys. Res., 65, 3931–3950, 1960.

Seppälä, A., Verronen, P. T., Clilverd, M. A., Randall, C. E., Tamminen, J., Sofieva, V., Backman, L., and Kyrölä, E.: Arctic and Antarctic polar winter NO_x and energetic particle precipitation in 2002–2006, Geophys. Res. Lett., 34, 12 810–+, doi:10.1029/2007GL029733, 2007.

Seppälä, A., Randall, C. E., Clilverd, M. A., Rozanov, E., and Harvey, V. L.: A Connection between geomagnetic activity and surface air temperature variability?, Geophys. Res. Lett., sumbitted, 2008.

Shimazaki, T.: Minor Constituents in the Middle Atmosphere, no. 6 in Developments in Earth and Planetary Physics, D. Reidel Publishing Company, 1984.

Stubbe, P.: Review of ionospheric modification experiments at Tromsø, J. Atmos. Terr. Phys., 58, 349–368, 1996.

Stubbe, P. and Varnum, W. S.: Electron energy transfer rates in the ionosphere, Planet. Space Sci., 20, 1121–+, 1972.

Stubbe, P., Kopka, H., Thidé, B., and Derblom, H.: Stimulated Electromagnetic Emission: A New Technique to Study the Parametric Decay Instability in the Ionosphere, J. Geophys. Res., 89, 7523–7536, 1984.

Tellegen, B. D. H.: Interaction between Radio-Waves?, Nature, 131, 840, doi: 10.1038/131840a0, 1933.

Tobiska, W., Woods, T., Eparvier, F., Viereck, R., Floyd, L., Bouwer, D., Rottman, G., and White, O.: The SOLAR2000 empirical solar irradiance model and forecast tool, J. Atmos. Sol.-Terr. Phys., 62, 1233–1250, 2000.

Verronen, P.: Effects of energetic particle precipitation events on mesospheric neutral chemistry, no. 54 in Geofysikaalisia julkaisuja (Geophysical publications), Finnish meteorological institute, Helsinki, Finland, ph.Lic. thesis, 2001.

Verronen, P. T.: Ionosphere-atmosphere interaction during solar proton events, Ph.D. thesis, Finnish Meteorological Institute, Helsinki, Finland, URL `http://ethesis.helsinki.fi/`, ISBN: 951-697-650-6, 2006.

Verronen, P. T., Seppälä, A., Clilverd, M. A., Rodger, C. J., Kyrölä, E., Enell, C.-F., Ulich, T., and Turunen, E.: Diurnal variation of ozone depletion during the October–November 2003 solar proton event, J. Geophys. Res., 110, A09S32, doi: 10.1029/2004JA010932, 2005.

Verronen, P. T., Ulich, T., Turunen, E., and J., R. C.: Sunset transition of negative charge in the D-region ionosphere during high-ionization conditions., Ann. Geophys., 24, 187–202, 2006.

Virtanen, I. I., Lehtinen, M. S., Nygren, T., Orispaa, M., and Vierinen, J.: Lag profile inversion method for EISCAT data analysis, Accepted for publication in Annales Geophysicae, 2007.

Wannberg, G., Wolf, I., Vanhainen, L.-G., Koskenniemi, K., Röttger, J., Postila, M., Markkanen, J., Jacobsen, R., Stenberg, A., Larsen, R., Eliassen, S., Heck, S., and Huuskonen, A.: The EISCAT Svalbard radar: A case study in modern incoherent scatter radar system design, Radio Sci., 32, 2283–2307, 1997.